The Relationship Between Cloud Radiative Effect and Surface Temperature Variability at ENSO Frequencies in CMIP5 Models

Nicholas J. Lutsko[1]

[1]Department of Earth, Atmospheric, and Planetary Sciences, Massachusetts Institute of Technology, Cambridge, Massachusetts

Key Points:

- Low clouds dominate the relationship between clouds and surface temperatures at ENSO frequencies.
- This is due to the thermodynamic variability of low clouds and not to changes in the large-scale dynamics.
- The cloud radiative effect by low clouds during ENSO events is well correlated with models' sensitivities.

Corresponding author: Nicholas Lutsko, `lutsko@mit.edu`

Abstract

The relationship between the cloud radiative effect (CRE) and surface temperature variability on ENSO time-scales is investigated in pre-industrial control simulations from the CMIP5 archive. The CRE is binned according to the mid-tropospheric vertical velocities and then regressed in frequency space versus tropical-mean surface temperatures. Low clouds play a leading role in the relationship between clouds and surface temperature variability, amplifying ENSO-induced surface temperature anomalies through thermodynamically-driven changes in the short-wave CRE. Changes in CRE driven by changes in the large-scale dynamics do not have a major influence on surface temperature variability. It is shown that the regression co-efficients between the CRE in subsiding regions and regions of weak ascent, and tropical-mean surface temperatures on ENSO frequencies are well correlated with models' climate sensitivities, constituting a potential "emergent constraint" on climate sensitivity.

1 Introduction

There is a well established connection between ENSO events and global-mean surface temperature (GMST), with El Niño events causing an increase in GMST and La Niña events causing a decrease. The changes in GMST are primarily driven by sea surface temperature (SST) anomalies in the tropical Pacific, which warm or cool the entire troposphere above them depending on the phase and amplitude of the ENSO event. These signals are then rapidly communicated to other regions of the tropical troposphere, since the tropical atmosphere cannot sustain large temperature gradients [*Sobel and Bretheron*, 2000]. The warming or cooling of surface temperatures outside the tropical Pacific is more complex however, as the strength of the coupling of the SSTs to the free troposphere above them has significant regional variations and so the surface temperatures of certain regions in the Indian and Atlantic oceans are not well correlated with ENSO variability [*Chiang and Sobel*, 2002].

Clouds also play a role in the response of GMST to ENSO events, and their net effect on ENSO is determined by a complex interplay between reductions in low cloud cover in regions of mean subsidence and increases in convective cloudiness in regions of mean ascent (e.g., *Klein and Hartmann* [1993]; *Bony et al.* [1997]; *Park and Leovy* [2004]), with the former amplifying surface temperature variability and the latter reducing it.

Because of the two effects partly cancel each other, it has proven difficult to untangle their relative contributions, though *Lloyd et al.* [2012] showed that the low cloud effect is the primary contributor to the difference between model feedbacks onto ENSO and those seen in observations.

Since low clouds are the source of much of the intermodel spread in Equilibrium Climate Sensitivity (ECS; e.g., *Vial* [2013]), it is tempting to use their ENSO-induced variability to constrain their forced changes. However recent work has shown that cloud feedbacks are highly sensitive to the pattern of surface temperature change (*Andrews et al.* [2015]; *Zhou et al.* [2017]; *Silvers et al.* [2018]; *Andrews and Webb* [2018]), in particular whether the warming is focused in regions of mean ascent or in regions of mean subsidence (or in the extratropics). This is problematic for attempts to constrain forced changes in clouds from ENSO-induced changes, as the patterns of low cloud changes during ENSO events differ from what is seen in forced simulations (*Zhu et al.* [2007]). On the other hand, there is statistical evidence that cloud feedbacks on unforced variability are related to forced cloud feedbacks (*Zhou et al.* [2015]; *Colman and Hanson* [2017]), so we cannot rule out the possibility that ENSO-induced cloud changes could be used to infer how clouds would be expected to change in a warmer world.

This study addresses these two questions – the relationships between different cloud types and tropical surface temperatures, and whether cloud changes on ENSO time-scales can be used to infer forced cloud changes – by applying two analysis techniques to data from the pre-industrial control simulations in the fifth Climate Model Intercomparison Project (CMIP5) archive. The first of these is binning the cloud radiative effect (CRE) based on the pressure velocity at 500hPa (ω) of each grid point, following the work of Bony and co-authors (e.g., *Bony et al.* [2004]; *Bony and Dufresne* [2005]). This is a commonly used technique for assessing the contribution of different cloud types to forced cloud changes in climate models (e.g., *Bony et al.* [2004]; *Bony and Dufresne* [2005]; *Wyant et al.* [2006]; *Zhao et al.* [2016]; *Byrne and Schneider* [2018]), and here permits the contribution of different cloud types to surface temperature variability on ENSO time-scales to be quantified.

The second technique is frequency-dependent regressions, which *Lutsko and Takahashi* [2018] used to study the relationship between TOA fluxes and surface temperatures in data from the pre-industrial control simulations in the CMIP5 archive (see also

MacMynowski et al. [2011]). A frequency-dependent "sensitivity" can be defined for these unforced simulations using the regression co-efficients between CRE and surface temperature, and a strong correlation was found across models between these regression co-efficients and the models' ECS values on time-scales of 2.5 to 3 years. This constitutes a potential "emergent constraint" between the behavior of clouds on ENSO time-scales and models' responses to increased CO_2 concentrations, though it was found that roughly 100 years of data are required for a strong relationship to emerge.

Besides the regression co-efficients, the frequency-dependent regressions also provide information about the relative phase of the CRE and surface temperature. It was found that, in the ensemble-median, the CRE is approximately 90° out of phase with tropical surface temperatures on ENSO frequencies. Naively, this implies that tropical clouds force surface temperature variability on these time-scales, but based on previous studies of the relationship between clouds and tropical surface temperatures on ENSO time-scales (*Klein et al.* [1999]; *Lau and Nath* [2001]; *Zhu et al.* [2007]; *Zhou et al.* [2017]), Lutsko and Takahashi suggested instead that tropical clouds rapidly respond to SST anomalies in the equatorial Pacific and then amplify tropical-mean surface temperature anomalies generated by the local SST anomalies during to ENSO events.

Building on this work, the CRE in the pre-industrial control simulations is here decomposed into ω bins and then regressed in frequency space versus tropical-mean surface temperatures. This permits the relationships between different cloud types and tropical surface temperatures to be investigated as a function of frequency, though the focus here is on ENSO time-scales ($\sim$2-5 years). This decomposition can also be used to identify which cloud-types are responsible for the relationship between the regression co-efficients and the models' sensitivities. A strong correlation across models is found between the changes in low cloud CRE on ENSO time-scales and the models' ECS values, which constitutes a stricter emergent constraint on Earth's ECS than that proposed by Lutsko and Takahashi.

After describing the data and methods used in the study in section 2, the relationship between tropical-mean surface temperature variability and thermodynamic changes in CRE (changes independent of changes in the large-scale dynamics) is investigated in section 3, then the relationship between tropical-mean surface temperature variability and variability in CRE due to changes in the large-scale dynamics is investigated in sec-

tion 4. Section 5 examines which cloud types are responsible for the relationship between the regression co-efficients and the models' ECS values seen by Lutsko and Takahashi, before conclusions are drawn in section 6.

2 Data and Methods

2.1 Data

The analysis used data from the pre-industrial control ("pi-control") experiments with 18 models participating in the CMIP5 project (Supplementary Table 1). 500 simulation years were used for each model and in cases where more than 500 years of data are available only the first 500 years were retained. The variables used in the analysis were the surface air temperature, the SSTs, the TOA outgoing long-wave radiation, the TOA outgoing short-wave radiation, the TOA outgoing clear-sky long-wave radiation and the TOA outgoing clear-sky short-wave radiation. The incoming solar radiation was assumed to be fixed and the total CRE was computed as the total flux minus the clear-sky flux. Similarly, the short-wave (long-wave) CRE was computed as the all-sky short-wave (long-wave) flux minus the clear-sky short-wave (long-wave) flux.

Estimates of the models' ECS values were taken from *Forster et al.* [2013] and *Geoffroy et al.* [2013]; except for the GFDL-CM3 and GFDL-ESM2G models, whose sensitivities were only estimated by *Forster et al.* [2013]; and the BNU-ESM model, whose sensitivity was only estimated by *Geoffroy et al.* [2013] (Supplementary Table 1). Comparisons were also made with estimates by the same authors of the models' feedback parameter β_F, where $ECS = F_{2xCO_2}/\beta_F$ and F_{2xCO_2} is the radiative forcing due to a doubling of CO_2 concentrations, and with estimates of the CRE-derived cloud feedback ($\beta_{F,cloud}$) from *Forster et al.* [2013].

Both studies estimated the β_F and ECS values from the 4xCO_2 experiments in the CMIP5 archive, but *Forster et al.* [2013] used the *Gregory et al.* [2004] method to estimate the values, whereas *Geoffroy et al.* [2013] estimated values as part of their iterative fitting of an energy balance model. The two sets of estimates are highly correlated, with an r^2 value of approximately 0.95. The *Forster et al.* [2013] estimates will be referred to as $\beta_{F,1}$ and ECS_1, and the *Geoffroy et al.* [2013] estimates as $\beta_{F,2}$ and ECS_2.

2.2 ω decomposition

Following Bony and co-authors (*Bony et al.* [2004]; *Bony and Dufresne* [2005]), the data were binned according to their monthly-mean 500hPa vertical pressure velocity, ω, with a bin-size of 5hPa (the results are not qualitatively sensitive to the choice of bin size), as a way of isolating different regimes of the large-scale overturning circulation. Only tropical (30°S to 30°N) data were included in the binning. After binning, annual-means were taken and the time-series were linearly de-trended to remove model drift (though note that some models have non-linear drift).

Tropical means can be taken by weighting the quantities in each bin by the probability density of that bin and then integrating over all bins. For instance, the tropical-mean surface temperature $\bar{T}$ is

$$\bar{T}(t) = \int_{-\infty}^{+\infty} P(t,\omega)T(t,\omega)d\omega, \tag{1}$$

where $P(t,\omega)$ is the distribution of ω, $T(t,\omega)$ is the mean surface temperature in that bin and t is measured in years. The ensemble-median values of the time-averaged probability densities, $[P(\omega)]$, are shown in the left panel of Figure 1.

The variability of the tropical-mean CRE ($\bar{C}(t)'$, where $\bar{C}(t)' = \bar{C}(t) - [\bar{C}]$) can be decomposed into a "dynamic" component due to $P(t,\omega)'$, a "thermodynamic" component due to $C(t,\omega)'$ and a non-linear component (*Bony et al.* [2004]; *Byrne and Schneider* [2018]):

$$\bar{C}'(t) = \int_{-\infty}^{+\infty} P(t,\omega)'[C(\omega)]d\omega + \int_{-\infty}^{+\infty} [P(\omega)]C(t,\omega)'d\omega + \int_{-\infty}^{+\infty} P(t,\omega)'C(t,\omega)'d\omega. \tag{2}$$

The dynamic term represents changes in the CRE due to large-scale circulation changes; for instance due to the re-organization of convection during ENSO events. The second term represents changes in cloud amount or in cloud radiative properties under fixed dynamic conditions, while the non-linear term represents co-variations of the dynamic and thermodynamic changes, and will be ignored hereafter.

The goal is to understand how different cloud-types are related to tropical-mean surface temperatures on ENSO time-scales and so the frequency-dependent regressions were performed between the tropical-mean surface temperatures ($\bar{T}'$) and the dynamic term, and between $\bar{T}'$ and the thermodynamic term.

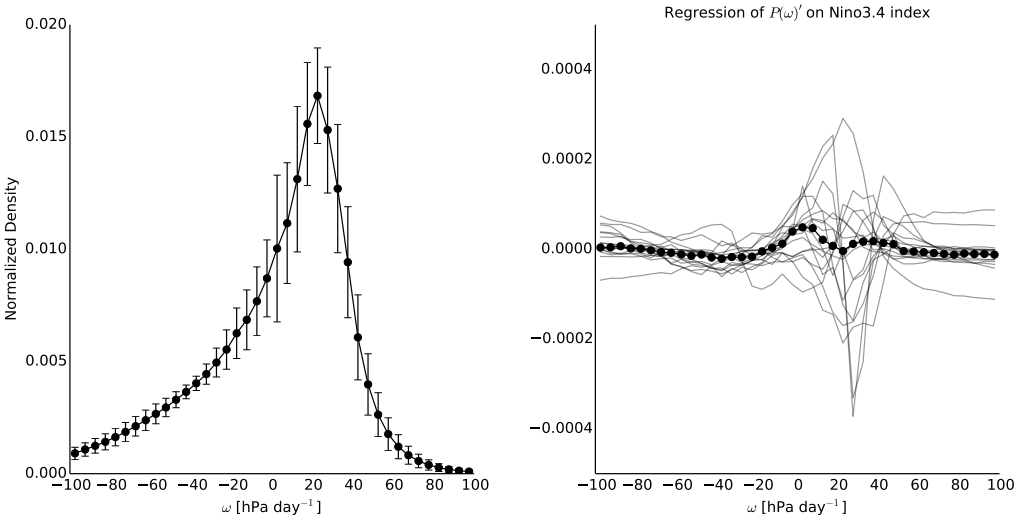

Figure 1. Left panel: Ensemble-median histogram of $[P(\omega)]$ for the 18 CMIP5 models analyzed in this study. The error bars show ±1 standard deviation. Right panel: Regression of $P(t,\omega)'$ onto the Nino3.4 index for each of the models used in the study (light gray lines). The thick line with the markers shows the ensemble-median of the regressions.

2.3 Spectral analysis

The spectral analysis follows the same procedure as *Lutsko and Takahashi* [2018], and is described in more detail in the Supplementary Text. The focus is on frequency-dependent regression co-efficients, which are calculated as

$$\tau(f) = \frac{C_{TR}(f)}{P_{TT}(f)}, \tag{3}$$

where f is frequency, P_{TT} is the power spectrum of global-mean surface temperature for a particular model and C_{TR} is the cross-spectrum of surface temperature with a particular TOA flux R. Since τ is complex it must be separated into its amplitude (a) and phase (ϕ):

$$a(f) = \frac{|C_{TR}(f)|}{P_{TT}(f)}, \tag{4}$$

$$\phi(f) = tan^{-1}\left[\frac{Im\{C_{TR}(f)\}}{Re\{C_{TR}(f)\}}\right], \tag{5}$$

where $\tau = ae^{i\phi}$. $a \geq 0$ and values of a will be referred to as "amplitudes" as a shorthand for "amplitudes of the regression co-efficients". The phase is always between -180° and 180°, with a phase of -180° being equivalent to a phase of 180°, and positive phases are taken to mean that the surface temperature leads the TOA flux.

The squared coherence was also estimated:

$$Coh^2_{TR}(f) = \frac{|C_{TR}(f)|^2}{P_{TT}(f)P_{RR}(f)}, \tag{6}$$

which gives a sense of the robustness of the relationship between R and T at a particular frequency.

3 Regressions Between Thermodynamic Variability and Tropical-Mean Surface Temperature

The results of the regressions between $C(\omega)'$ (the binned total CRE) and $\bar{T}'$ are summarized in Figure 2. The values shown are averaged over the 2.5 years^{-1} to 3 years^{-1} frequency band, since Lutsko and Takahashi demonstrated that this frequency band can be used to predict the models' sensitivities, however the results are similar using a wider range of frequencies in the ENSO range (Supplementary Figure 1). Individual model results are in light gray and the ensemble-median values are in black.

The coherence is generally low (0.2-0.4 in the ensemble-median), except for velocities between about -15hPa/day and 30hPa/day, where it reaches values of more than 0.6 in the ensemble median at 5hPa. The phase is close to +90° in the ensemble-median at most frequencies but there is a large intermodel spread, except for between about -5hPa/day and 30hPa/day, when all but two of the models are close to +90°. The amplitudes a are small everywhere except between -15hPa/day and 30hPa/day, and there is a maximum at 10hPa/day of about 0.06 Wm^{-2}K^{-1}.

As in Lutsko and Takahashi, the 90° phase difference for the regions of weak ascent and of subsidence can be interpreted as representing clouds amplifying ENSO-induced surface temperature anomalies. For instance, during warm El Niño events low cloud cover is reduced, amplifying the warming of tropical-mean surface temperatures. Supplementary Figure 2 supports this interpretation by showing lag-regressions between the CRE averaged over bins 0 to 40hPa/day and tropical-mean surface temperatures (top left panel); between the CRE in these regions and the Nino3.4 index in the models (top right panel); between the Nino3.4 index and tropical-mean surface temperatures (bottom left panel) and between the CRE averaged over bins 0 to 40hPa/day and tropical-mean cloud cover (bottom right panel). Note that linearly de-trended, monthly data were used to estimate these lag-regressions.

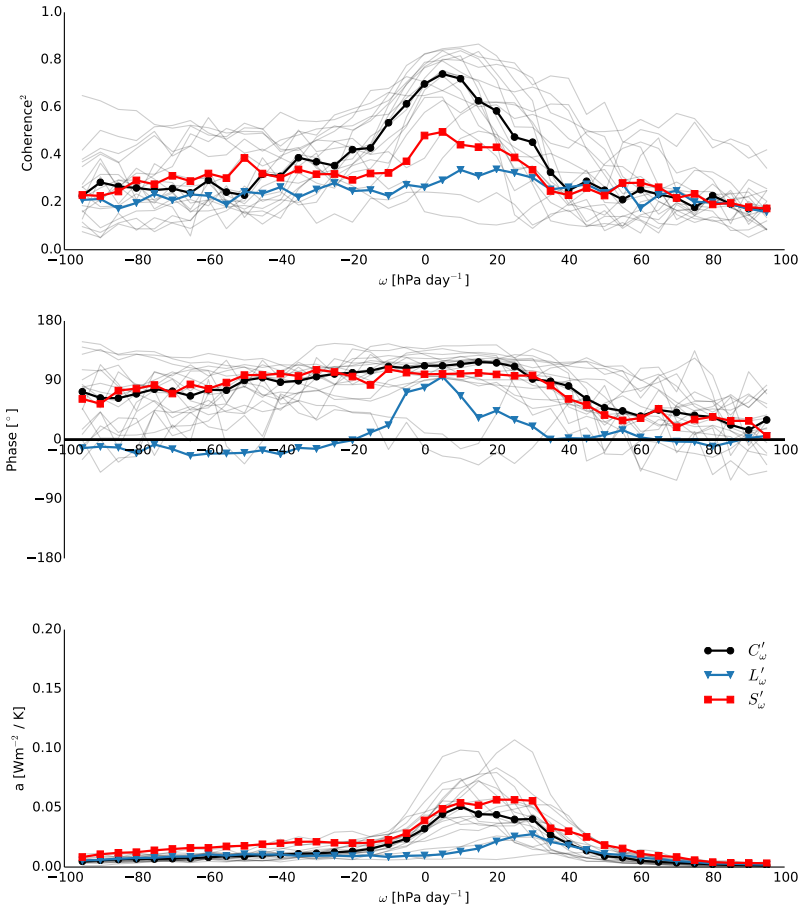

Figure 2. Top panel: squared-coherence between $\bar{T}'$ and $C(\omega)'$ for ω between -100hPa/day and 100hPa/day, averaged over frequencies of 2.5 years^{-1} to 3 years^{-1}. The individual models are in gray and the ensemble median is shown by the thick black line. The ensemble-median coherences for the regressions with the long-wave CRE ($L(\omega)'$) and the short-wave CRE ($S(\omega)'$) are shown in the thick blue and red lines, respectively. Middle panel: same but for the phase between $\bar{T}'$ and $C(\omega)'$. Positive phase means that surface temperature leads the TOA flux, though if two variables are $\pm 90°$ out of phase then either one variables forces the other or one variable damps the other. For instance, the phase will be $+90°$ if $\bar{T}' = dC(\omega)'/dt$ or if $d\bar{T}'/dt = -C(\omega)'$. Bottom panel: same but the amplitudes between $\bar{T}'$ and $C(\omega)'$ are shown.

In line with the interpretation given above, the CRE is approximately in phase with the Nino3.4 index, and is anti-correlated with it, with a minimum correlation of around -0.4 in the ensemble-median. The CRE is also anti-correlated with tropical-mean temperature, but leads this by about four months in the ensemble-median. As expected, the

Nino3.4 index is strongly correlated (co-efficient of about 0.9) with tropical-mean surface temperature, and leads this by about three months in the ensemble-median. These relationships support the claim that the low cloud CRE quickly responds to ENSO-induced SST anomalies in the equatorial Pacific and then amplifies tropical-mean surface temperature anomalies, which lag by several months. The CRE in subsiding regions is highly correlated with tropical-mean low cloud cloud cover, suggesting that the low cloud CRE variability is mainly due to changes in tropical cloud cover (as opposed to changes in cloud thickness or depth).

The blue and red lines in Figure 2 show the results for the regressions with the long-wave and short-wave CREs ($L(\omega)'$ and $S(\omega)'$, respectively) with only the ensemble-median values shown for clarity. The regressions for $S(\omega)'$ generally resemble the $C(\omega)'$ regressions: the phase is always near 90° and the values of a are very similar, though they peak at about 30hPa/day instead of at 10hPa/day. The coherence is weaker than for the total CRE, with a maximum of about 0.5 at 5hPa/day. It is unclear why adding the long-wave CRE makes the total CRE in these bins more coherent with surface temperature.

In contrast, there is little resemblance between the long-wave regressions and the total CRE regressions. The phase is always close to zero, except for a few values at velocities close to 0hPa/day when it approaches +90°. There is a small peak in the amplitudes at about 30hPa, but otherwise the amplitudes are small, while the coherence is weak for all bins. This peak in regions of strong subsidence is unexpected, since these regions are dominated by low clouds, which have a weak long-wave effect, and the long-wave amplitudes appear to actually cancel the short-wave amplitudes somewhat, so that the amplitudes for the total CRE are largest in regions of relatively weak subsidence.

In the ensemble-median, the longwave CRE is roughly in phase with $\bar{T}'$ in these regions of strong subsidence, suggesting that it is acting as a negative feedback on temperature variability. But as Supplementary Figure 3 shows, this phase is the result of cancellation between a wide spread in phases across the individual models, making it difficult to interpret the reason for this peak. Lag correlations are also inconclusive, as the correlation between the low cloud long-wave CRE and tropical-mean surface temperature is very weak (not shown). Clarifying the effect of the long-wave CRE of low clouds on surface temperature variability will require focused modelling work, and is left for future work.

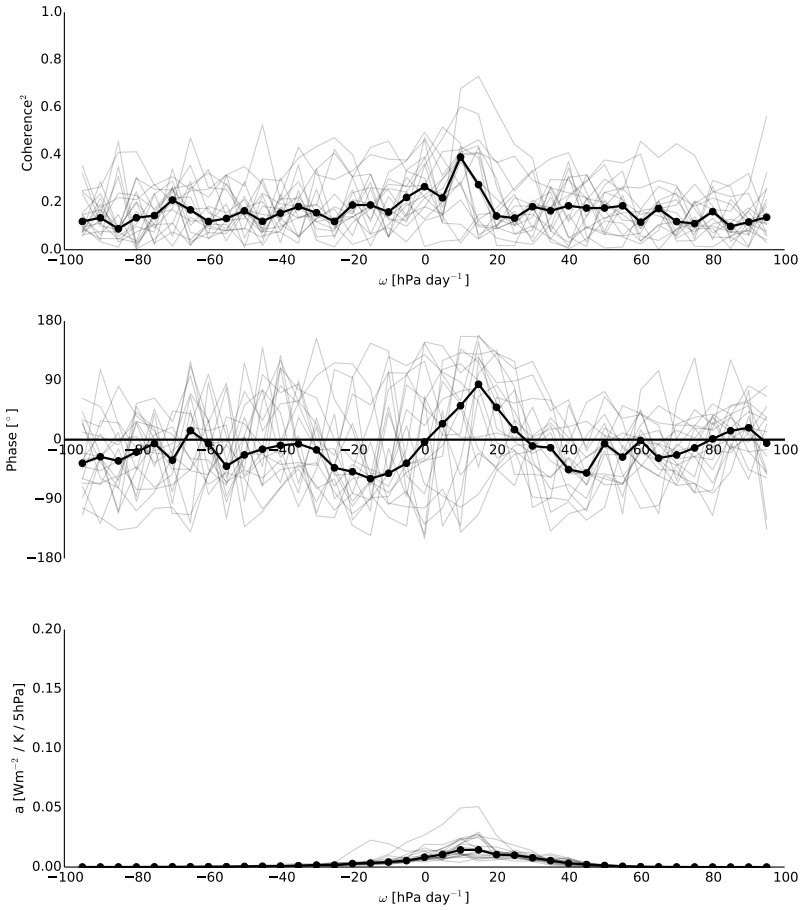

Figure 3. Same as Figure 2 but for the regressions between $P(\omega)'$ and $\bar{T}'$.

4 Regressions Between Dynamic Variability and Tropical-Mean Surface Temperature

Figure 3 repeats Figure 2, but for the regressions between $P(\omega)'$ and $\bar{T}'$. The relationship between these is weak, as the coherence and amplitude are both low at almost all frequencies and there is much intermodel spread in the coherence and the phase. There is a weak peak in the amplitudes and in the coherence at about 10hPa/day, however, and the phase is close to 90° in the ensemble median at 10hPa/day. So although the dynamic variability is in general not an important component of the relationship between cloud fluxes and surface temperature variability on ENSO time-scales, it may play a role in regions of weak subsidence.

The minor role of dynamics in driving CRE variability is partly explained by the right panel of Figure 1, which shows the regressions of $P(\omega)'$ onto the Nino3.4 index for

each model. The regressions exhibit very different behaviors across the models: in some models $P(\omega)'$ is enhanced between about 0 and 40hPa/day and reduced everywhere else, while in other models there is a shift in the distribution, as $P(\omega)'$ is reduced in regions of weak subsidence and enhanced in regions of strong subsidence. In all of the models, however, the largest values of the projections are only 1-5% of the climatological values of $[P(\omega)]$. This implies that although there may be considerable re-organization of the convection in space during ENSO events, the relative fractions of the different regimes do not exhibit large temporal variations in the models, and tropical-mean surface temperatures are only weakly affected by CRE variability due to dynamic changes.

5 Comparing with Climate Sensitivity Estimates

As in Lutsko and Takahashi, the amplitudes can be thought of as frequency-dependent internal variability sensitivities, and so regressing them against the models' climate sensitivities is a way of investigating whether the models' internal variability is correlated with their sensitivities to external forcing. This is shown in Figure 4, which plots the r^2 values for correlations between the amplitudes for $C(\omega)'$, averaged over the 2.5 to 3 years^{-1} frequency bands, and the estimates of the models' β_F and ECS values.

The strongest correlations are in the -10hPa to 25hPa bins, with r^2 values of up to 0.6, and are weaker with the ECS estimates than with the β_F estimates. Decomposing into the short-wave and long-wave components demonstrates that most of this correlation comes from the short-wave (bottom panel of Figure 4), though adding the long-wave improves the relationship somewhat. Plotting the values of $a(f, \omega)$, averaged over the 0 to 20hPa/day bins, against the sensitivity estimates shows that models with larger values of a have larger climate sensitivities (smaller values of β_F) (Supplementary Figure 4). That is, models in which clouds in regions of weak subsidence and weak ascent amplify tropical mean surface temperature variability more strongly on ENSO time-scales are more sensitive to external forcings. Intuitively, this is what we would expect: models which experience a larger reduction in low clouds when tropical surface temperatures warm have larger climate sensitivities.

Similar results are obtained when the correlations are performed with the $\beta_{F,cloud}$ estimates (Supplementary Figure 5); while the amplitudes from the regressions with $P(\omega)'$

are not well correlated with the sensitivity estimates (Supplementary Figure 6), as expected from the previous section.

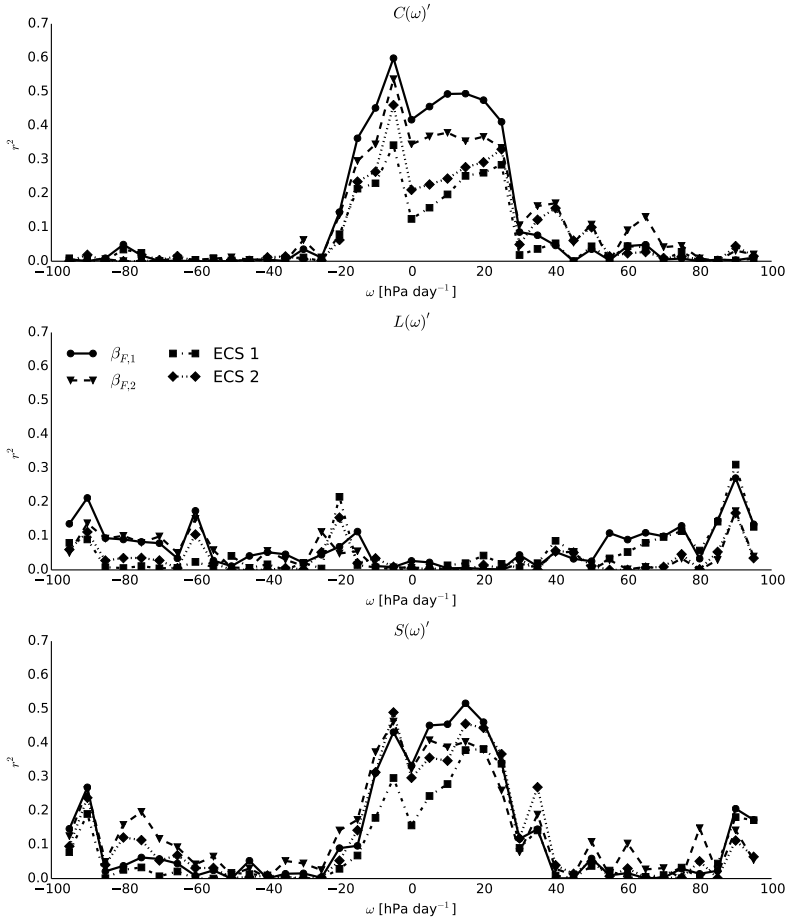

Figure 4. Top panel: r^2 values for regressions between the four sets of sensitivity estimates and the amplitudes, averaged over frequencies of 2.5 years^{-1} to 3 years^{-1}, for the regressions between $\bar{T}'$ and $C(\omega)'$. Middle panel: same for the regressions between $\bar{T}'$ and $L(\omega)'$. Bottom panel: same for the regressions between $\bar{T}'$ and $S(\omega)'$.

6 Conclusion

The results presented here demonstrate that the relationship between tropical-mean surface temperature variability and the CRE on ENSO time-scales is dominated by the thermodynamic variability of clouds in subsiding regions and regions of weak ascent ($\omega \sim -10$ to 30hPa/day). This variability is 90° out of phase with surface temperature, and amplifies ENSO-induced surface temperature variability through reductions (enhance-

ments) of low cloud cover during warm (cold) El Niño (La Niña) events (see also *Klein et al.* [1999]; *Lau and Nath* [2001]; *Zhu et al.* [2007]; *Zhou et al.* [2017]). A caveat to this picture is that the long-wave CRE of clouds in regions of strong subsidence ($\geq$ 20hPa/day) partly cancels these clouds' short-wave CRE, so that the total CRE in these regions has a smaller effect on surface temperature variability than clouds in regions of weaker descent. It is difficult to determine why the long-wave CRE in regions of strong subsidence has this effect because of the large intermodel spread in the phase. In general CRE variability due to changes in the large-scale dynamics during ENSO events does not impact surface temperature variability, despite the substantial re-organization of convection in space during ENSO events, though it does seem to play a minor role in regions of weak subsidence ($\sim$10hPa/day).

The frequency-dependent regression coefficients for the regressions between the total CRE in subsiding regions and regions of weak ascent, and tropical-mean surface temperatures are well correlated ($r^2 > 0.6$) across models with the models' sensitivities (Figure 4), with larger regression coefficients corresponding to models with larger climate sensitivities (Supplementary Figure 4). In other words, models which experience larger reductions (enhancements) of low cloud cover during warm (cold) El Niño (La Niña) events have larger ECS values. Previous studies have emphasized the role of clouds in regions of strong subsidence for the intermodel spread in climate sensitivity (e.g., *Bony and Dufresne* [2005]; *Vial* [2013]), but it has been found here that the behavior of these clouds on ENSO time-scales is less predictive of models' sensitivities. Part of the reason for this may be the behavior of the long-wave CRE noted above, while it is also possible that the CRE variability in regions of strong subsidence in unforced simulations is small compared with the CRE changes in forced simulations and so the internal variability may not sample the relevant parts of the phase space. This possibility has not been investigated here.

These results add to our picture of how clouds influence surface temperature variability on ENSO time-scales, and also constitute a stricter emergent constraint than that identified by Lutsko and Takahashi: constraining the relationship between clouds in subsiding regions and regions of weak ascent, and tropical-mean surface temperatures on ENSO time-scales can help us to constrain Earth's ECS. However, it has been shown previously that O(100 years) of data are needed to accurately characterize ENSO spectra (*Wittenberg* [2009]; *Lutsko and Takahashi* [2018]), suggesting that the emergent constraint developed here is of limited practical use for the near-term. Nevertheless, the results pre-

sented above demonstrate that, despite the substantial differences in the patterns of cloud changes during ENSO events and in response to increased CO_2 concentrations, there is a strong relationship across models between the CREs resulting from these cloud changes. This relationship is worth exploring further, through focused modelling studies as well as through observational investigations of how ENSO-induced changes in Earth's CRE influence ENSO-induced tropical surface temperature anomalies.

Acknowledgments

I thank Max Popp, Cristian Proistosescu, Mike Byrne and Paul O'Gorman for helpful conversations and comments on earlier versions of this manuscript, as well as the NSF for supporting me through grant AGS-1623218, "Collaborative Research: Using a Hierarchy of Models to Constrain the Temperature Dependence of Climate Sensitivity". The CMIP5 data can be accessed at https://cmip.llnl.gov/cmip5/data_portal.html and the scripts used in this analysis are available at https://github.com/nicklutsko/CMIP5_ENSO/.

References

Andrews, T., and M. J. Webb (2018), The dependence of global cloud and lapse rate feedbacks on the spatial structure of tropical pacific warming, *Journal of Climate*, *31*(7), 641–654.

Andrews, T., J. M. Gregory, and M. J. Webb (2015), The dependence of radiative forcing and feedback on evolving patterns of surface temperature change in climate models., *Journal of Climate*, *28*(2), 1630–1648.

Bony, S., and J. L. Dufresne (2005), Marine boundary layer clouds at the heart of tropical cloud feedback uncertainties in climate models., *Geophysical Research Letters*, *32*(6), L20,806.

Bony, S., K. M. Lau, and Y. C. Sud (1997), Sea surface temperature and large-scale circulation influences on tropical greenhouse effect and cloud radiative forcing., *Journal of Climate*, *10*(6), 2055–2077.

Bony, S., J. L. Dufresne, H. L. Treut, J. J. Morcrette, and C. Senior (2004), On dynamic and thermodynamic components of cloud changes, *Climate Dynamics*, *22*(6), 71–86.

Byrne, M. P., and T. Schneider (2018), Atmospheric dynamics feedback: Concept, simulations and climate implications., *Journal of Climate*, p. Accepted.

Chiang, J. C. H., and A. H. Sobel (2002), Tropical tropospheric temperature variations caused by enso and their influence on the remote tropical climate, *Journal of Climate*, *15*(9), 2616–2631.

Colman, R. A., and L. I. Hanson (2017), On the relative strength of radiative feedbacks under climate variability and change., *Climate Dynamics*, *40*(1), 1–15.

Forster, P. M., T. Andrews, P. Good, J. M. Gregory, L. S. Jackson, and M. Zelinka (2013), Evaluating adjusted forcing and model spread for historical and future scenarios in the cmip5 generation of climate models, *Journal of Geophysical Research: Atmospheres*, *118*, 1139–1150.

Geoffroy, O., D. Saint-Martin, G. Bellon, A. Voldoire, D. J. L. Olivie, and S. Tyteca (2013), Transient climate response in a two-layer energy-balance model. part ii: Representation of the efficacy of deep-ocean heat uptake and validation for cmip5 aogcms, *Journal of Climate*, *26*(6), 1859–1876.

Gregory, J. M., W. J. Ingram, M. A. Palmer, G. S. Jones, P. A. Stott, R. B. Thorpe, J. A. Lowe, T. C. Johns, and K. D. Williams (2004), A new method for diagnosing radiative forcing and climate sensitivity, *Geophysical Research Letters*, *31*, L03205.

Klein, S. A., and D. L. Hartmann (1993), The seasonal cycle of low stratiform clouds, *Journal of Climate*, *6*(6), 1587–1606.

Klein, S. A., B. J. Soden, and N.-C. Lau (1999), Remote sea surface temperature variations during enso: Evidence for a tropical atmospheric bridge, *Journal of Climate*, *12*(6), 917–932.

Lau, N.-C., and M. J. Nath (2001), Impact of enso on sst variability in the north pacific and north atlantic: Seasonal dependence and role of extratropical seaair coupling, *Journal of Climate*, *14*(7), 2846–2866.

Lloyd, J., E. Guilyardi, and H. Weller (2012), The role of atmosphere feedbacks during enso in the cmip3 models. part iii: The shortwave flux feedback, *Journal of Climate*, *25*(6), 4275–4293.

Lutsko, N. J., and K. Takahashi (2018), What can the internal variability of cmip5 models tell us about their climate sensitivity?, *Journal of Climate*, *31*(13), 5051–5069.

MacMynowski, D. G., H. J., Shin, and K. Caldeira (2011), The frequency response of temperature and precipitation in a climate model, *Geophysical Research Letters*,

38(23), 2011GL16711.

Park, S., and C. B. Leovy (2004), Marine low-cloud anomalies associated with enso, *Journal of Climate*, *17*(6), 3448–3469.

Silvers, L. G., D. Paynter, and M. Zhao (2018), The diversity of cloud responses to twentieth century sea surface temperatures. *Geophysical Research Letters*, *45*, 391–400.

A. H. Sobel and C. S. Bretherton (2002), Modeling Tropical Precipitation in a Single Column, *Journal of Climate*, *13*(9), 4378–4392.

Vial J.,J.-L. Dufresne, and S. Bony (2013), On the interpretation of inter-model spread in cmip5 climate sensitivity estimates., *Climate Dynamics*, *41*(1), 3339–3362.

Wittenberg, A. T. (2009), Are historical records sufficient to constrain ENSO simulations? *Geophysical Research Letters*, *36*, 2011GL12702.

Wyant, M. C., C. S. Bretherton, J. T., Bacmeister, J. T., Kiehl, I. M., Held, M. Zhao, S. A. Klein, and B. J., Soden (2006), A comparison of low-latitude cloud properties and their response to climate change in three AGCMs sorted into regimes using mid-tropospheric vertical velocity., *Climate Dynamics*, *27*(23), 261–279.

Zhao, M., J. C. Golaz, I. M., Held, V. Ramaswamy, S. J. Lin, P. Ginoux, B. Wyman, L. J. Donner, D. Paynter and H. Guo (2016), Uncertainty in model climate sensitivity traced to representations of cumulus precipitation microphysics, *Journal of Climate*, *29*(23), 543–560.

Zhou, C., M. D. Zelinka, A. E. Dessler, and S. A. Klein (2015), The relationship between interannual and long-term cloud feedbacks, *Geophysical Research Letters*, *42*(23), 10,463–10,469, 2015GL066698.

Zhou, C., M. D. Zelinka, and S. A. Klein (2017), Analyzing the dependence of global cloud feedback on the spatial pattern of sea surface temperature change with a green's function approach, *Journal of Advances in Modeling Earth Systems*, *9*(23), 2174–2189.

Zhu, P., J. J. Hack, J. T. Kiehl, and C. S. Bretherton (2007), Climate sensitivity of tropical and subtropical marine low cloud amount to enso and global warming due to doubled co2, *Journal of Geophysical Research*, *112*(1), D17,108.